**Support Information**

# Fighting Immune Cold and Reprogramming Immunosuppressive Tumor Microenvironment with Red Blood Cell Membrane-Camouflaged Nanobullets

Zhe Yang[a], Di Gao[a], Xiaoqing Guo[a], Lin Jin[d], Juanjuan Zheng[b], Ying Wang[a], Shuojia Chen[a], Xuewei Zheng[a], Li Zeng[a], Ming Guo[c], Xingcai Zhang[b, c, *], Zhongmin Tian[a, *]

[a] *The Key Laboratory of Biomedical Information Engineering of Ministry of Education, School of Life Science and Technology, Xi'an Jiaotong University, Xi'an 710049, China*

[b] *John A. Paulson School of Engineering and Applied Sciences, Harvard University, Cambridge, Massachusetts 02138, United States*

[c] *School of Engineering, Massachusetts Institute of Technology, Cambridge, MA, 02139, United States*

[d] *International Joint Research Laboratory for Biomedical Nanomaterials of Henan, Zhoukou Normal University, Zhoukou 466001, P. R. China*

* Corresponding author

* E-mail: xingcai@mit.edu (Xingcai Zhang)

zmtian@xjtu.edu.cn (Zhongmin Tian)

## Table S1

**Table S1.** The molecular weight and PDI of the PAAV and PAAV-SNO copolymer.

| Polymer | Mw (g/mol) | PDI |
|---|---|---|
| PAAV | 11364 | 1.24 |
| PAAV-SNO | 12931 | 1.36 |

**Figure S1**

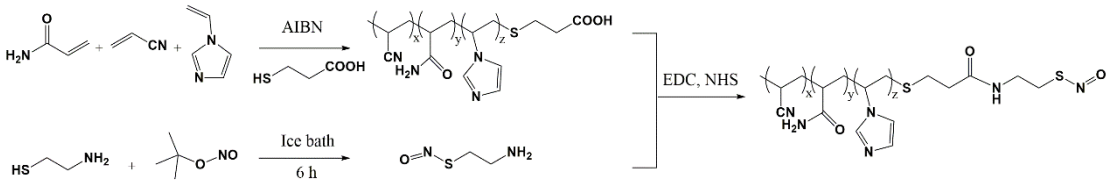


**Figure S1.** Synthesis of P(AAm-*co*-AN-*co*-VIm)-SNO copolymer (PAAV-SNO).

**Figure S2**

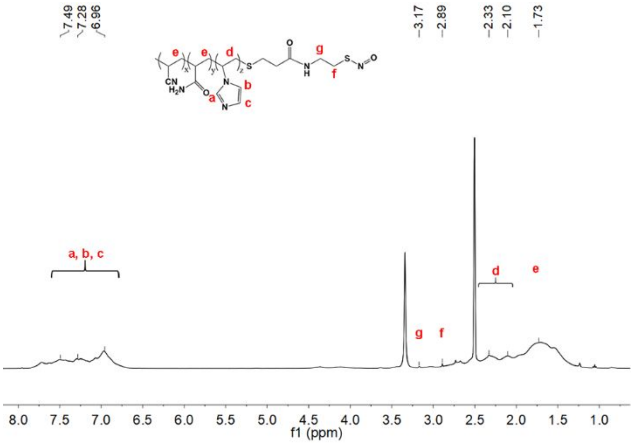


**Figure S2.** $^{1}$H-NMR spectrum ($d^{6}$-DMSO) of PAAV-SNO copolymer.

**Figure S3**

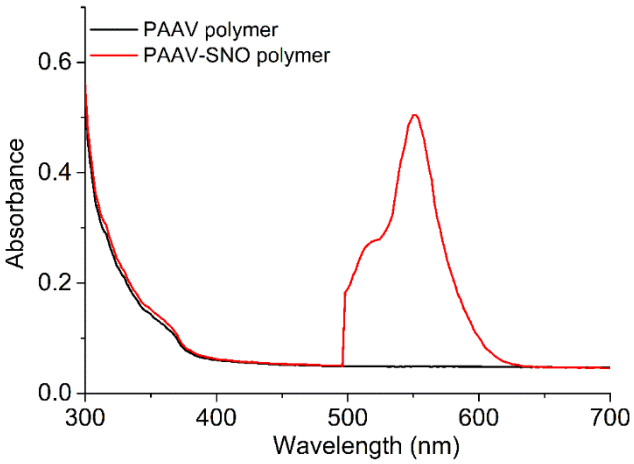


**Figure S3.** UV-VIS spectrum of PAAV polymer and PAAV-SNO polymer in DMSO.

**Figure S4**

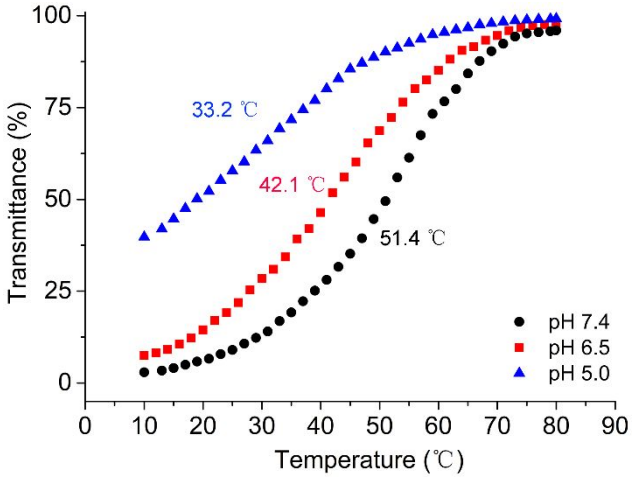


**Figure S4.** Turbidity heating profiles of PAAV-SNO aqueous solutions (0.5 mg/mL) at varying pH values of pH 7.4, 6.5 and 5.0.

**Figure S5**

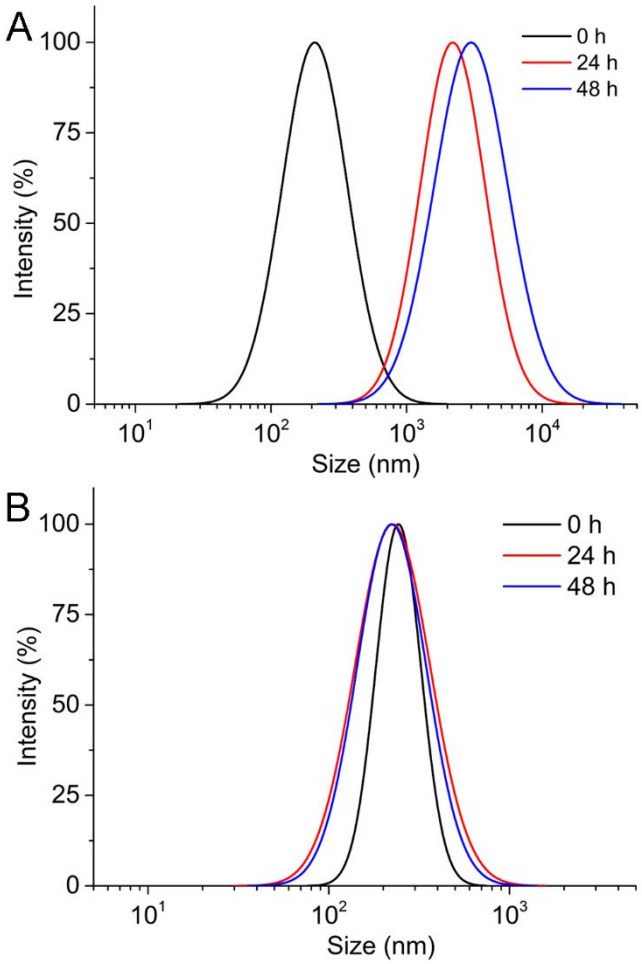


**Figure S5.** Size distribution of PAAV-SNO NPs and RBCm/PAAV-SNO NPs in PBS (pH 7.4, 0.01 M) containing 10% FBS at 37 ℃.

**Figure S6**

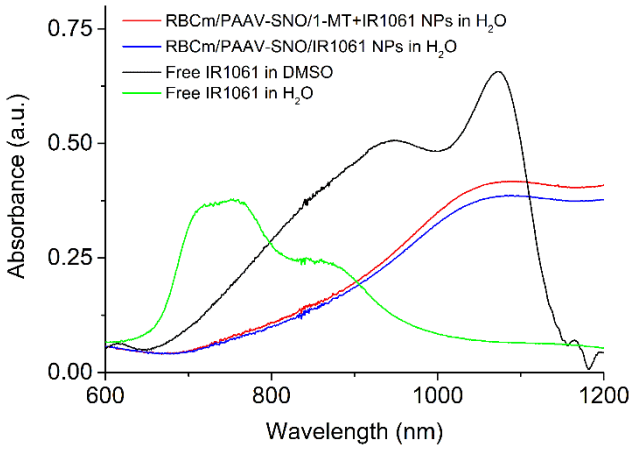


**Figure S6**. UV-VIS-NIR spectrum of different drug formulations in $H_2O$ and DMSO.

**Figure S7**

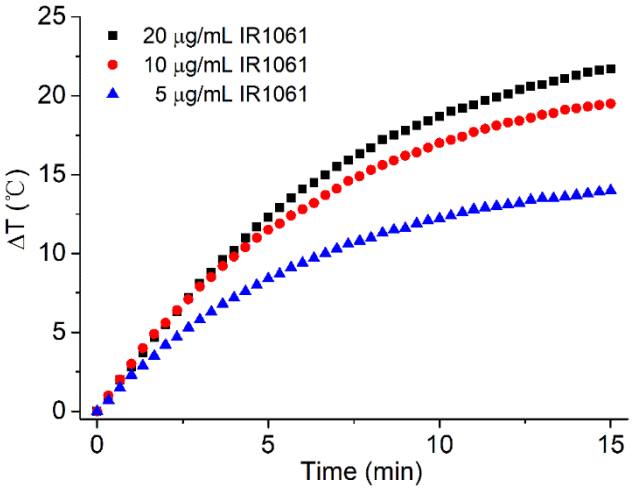


**Figure S7.** Temperature changes of RBCm/PAAV-SNO/1-MT+IR1061 NPs at different concentrations of IR1061 under 1064 nm laser irradiation (0.86 W/cm$^2$).

**Figure S8**

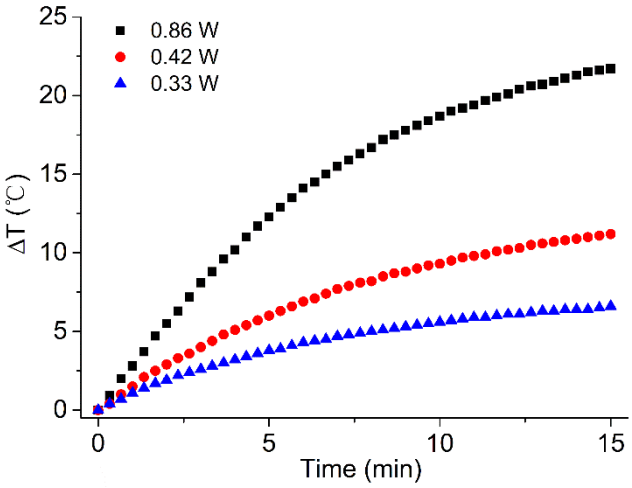


**Figure S8.** Temperature changes of RBCm/PAAV-SNO/1-MT+IR1061 NPs at 20 $\mu$g/mL of IR1061 under 1064 nm laser irradiation with different power densities.

**Figure S9**

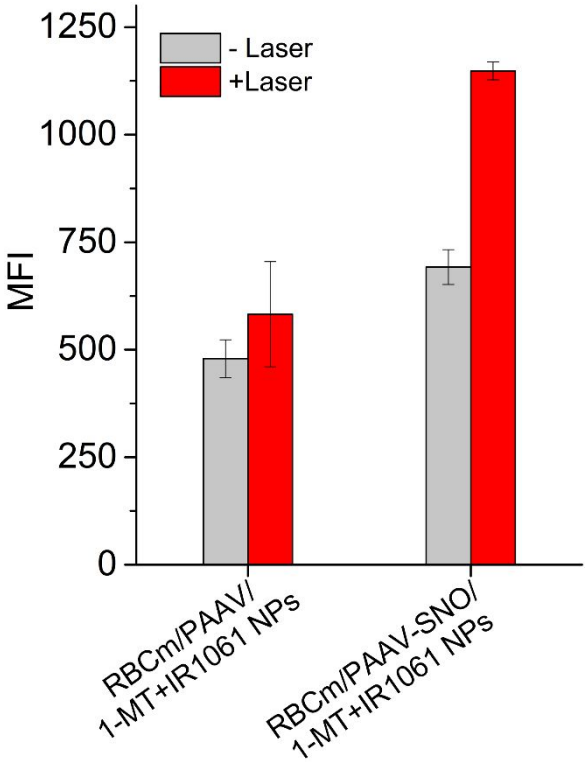


**Figure S9.** Flow cytometry analysis of intracellular NO in 4T1 cells after the treatment of RBCm/PAAV/IR1061+1-MT and RBCm/PAAV-SNO/IR1061+1-MT with or without 1064 nm laser irradiation (0.86 W/cm$^2$, 5 min) (n=4).

**Figure S10**

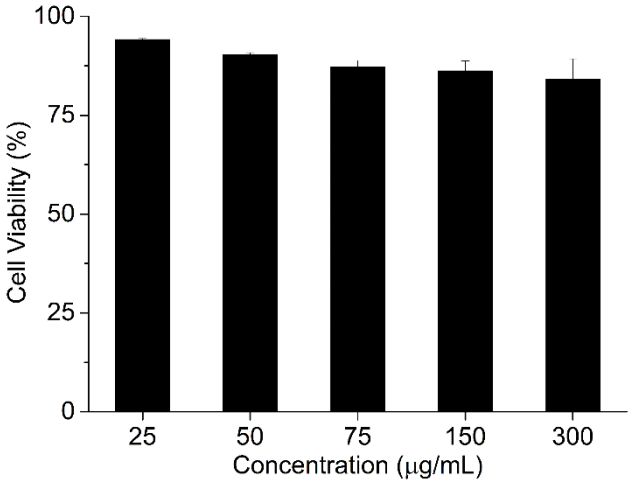


**Figure S10.** *In vitro* cytotoxicity of blank RBCm/PAAV-SNO NPs on 4T1 cell at different concentration (n=5).

**Figure S11**

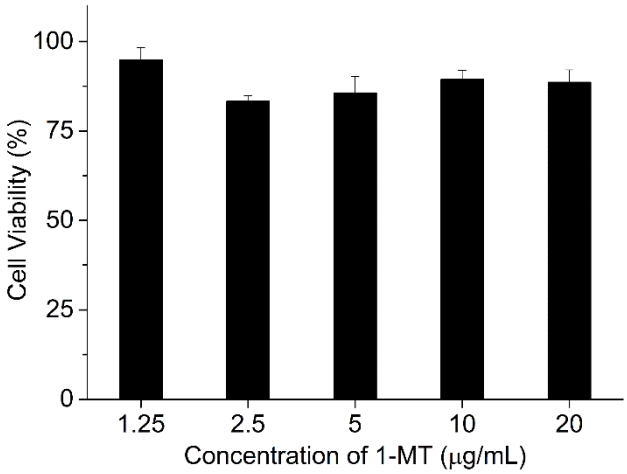


**Figure S11**. *In vitro* cytotoxicity of free 1-MT on 4T1 cell at different concentration (n=5).

## Figure S12

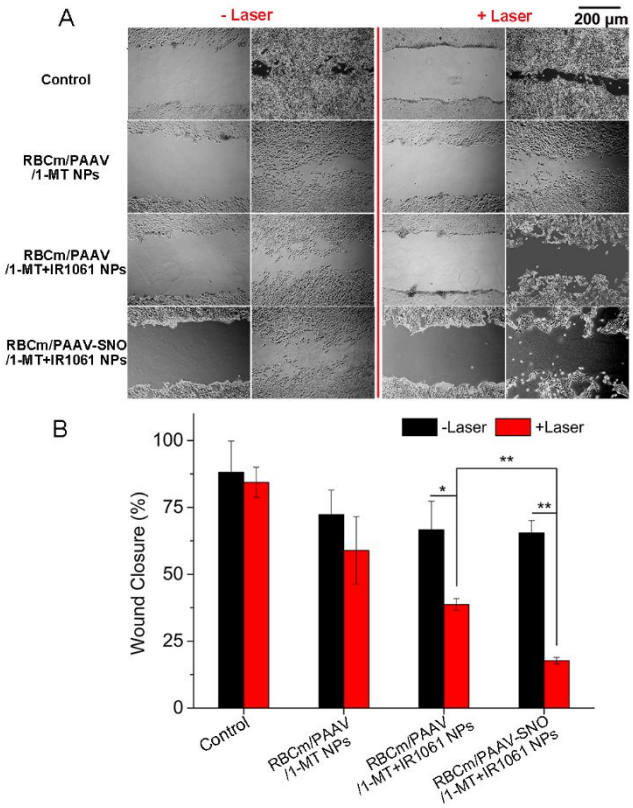


**Figure S12.** (A) Images and (B) quantification of 4T1 cells' wound-healing response after the treatment of different drug formulations with or without 1064 nm laser irradiation (0.86 W/cm$^2$, 5 min) (n=5).

**Figure S13**

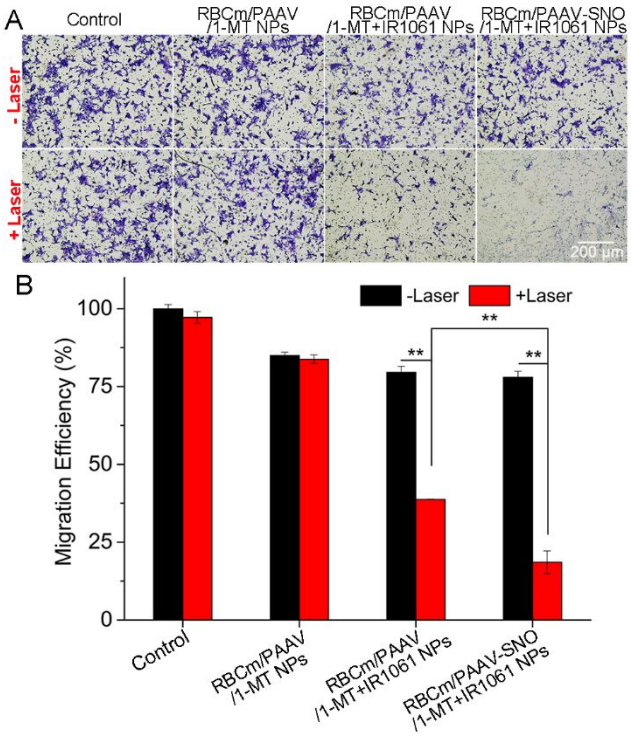


**Figure S13.** (A) Images and (B) quantification of transwell migration assay of 4T1 cells treated with varying drug formulations with or without 1064 nm laser irradiation (0.86 W/cm$^2$, 5 min) (n=5).

**Figure S14**

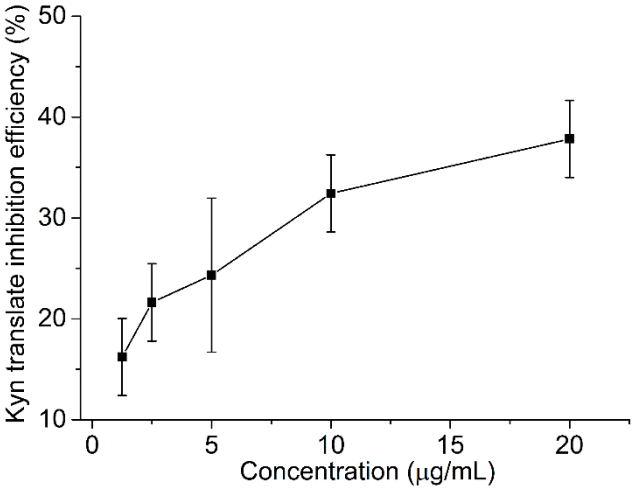


**Figure S14.** Kyn translate inhibition efficiency of 1-MT at different concentration in 4T1 cells (n=4).

**Figure S15**

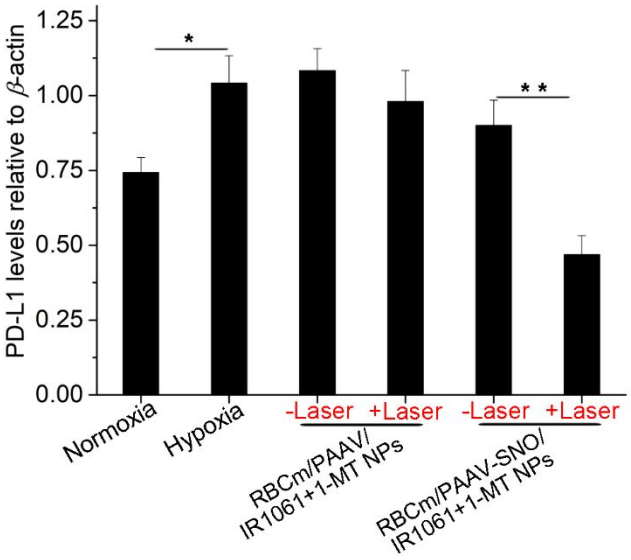


**Figure S15.** Western blot analysis and relative intensity of PD-L1 in 4T1 cells after the treatments of different drug formulations with or without 1064 nm laser irradiation (0.86 W/cm$^2$, 5 min) under normoxia or hypoxia condition (1% $O_2$). (n=3)

**Figure S16**

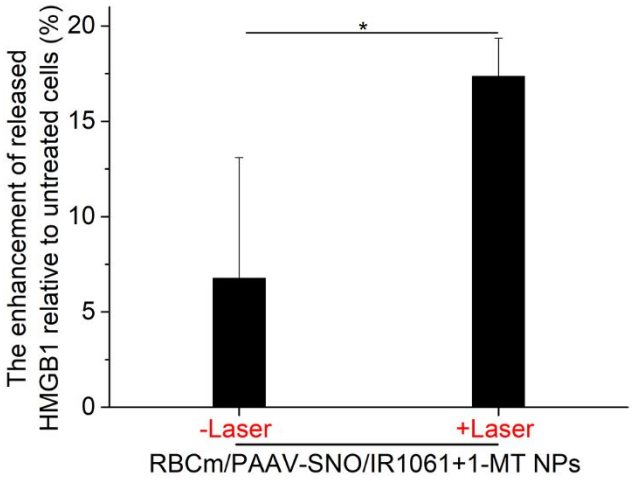


**Figure S16**. The enhancement percentage of released HMGB1 from 4T1 cells after the treatment of RBCm/PAAV-SNO/1-MT+IR1061 NPs with or without 1064 nm laser irradiation (0.86 W/cm$^2$, 5 min). (n=4)

**Figure S17**

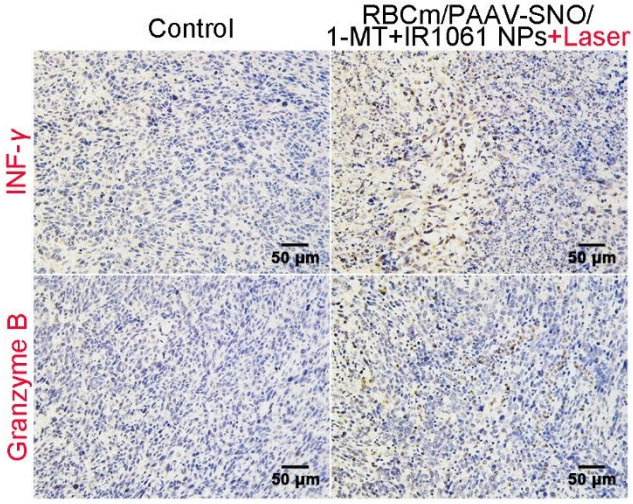


**Figure S17.** *In vivo* ICD effect of the treatment of RBCm/PAAV-SNO/1-MT+IR1061 NPs plus 1064 nm laser irradiation. IHC staining of INF-*γ* and Granzyme B in 4T1 tumor in the contralateral flank of the mice (n=5).

**Figure S18**

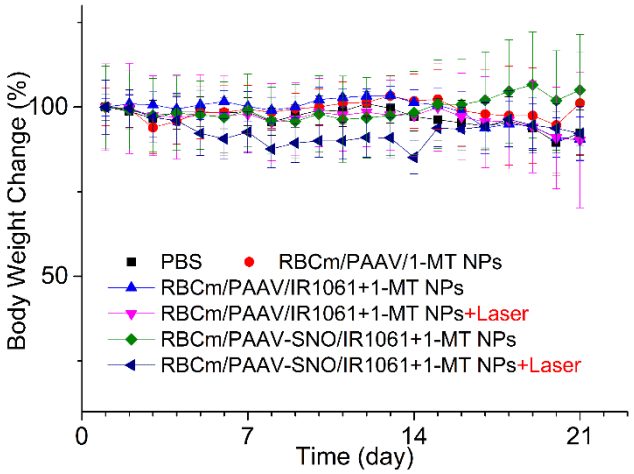


**Figure S18.** The changes in body weight during the experimental period (0~21 day) (n=6).

## Figure S19

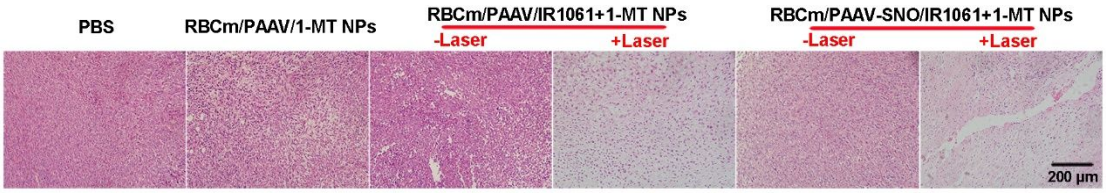


**Figure S19.** H&E staining analysis of tumor slices after different treatments.

**Figure S20**

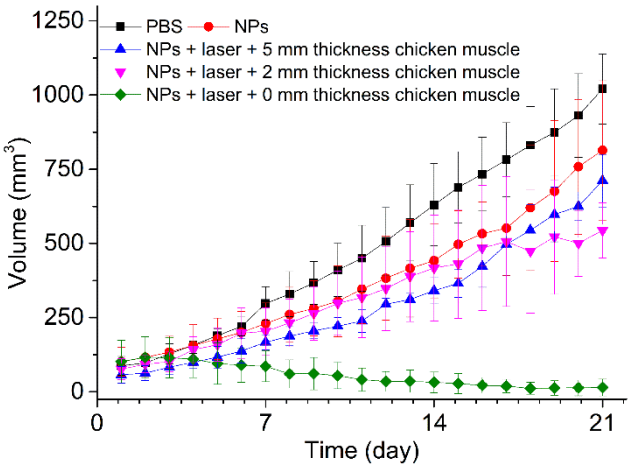


**Figure S20.** Tumor growth curves of different groups after treatment. And chicken breast muscles with varying thickness (0, 2 and 5 mm) were placed on the tumor tissues when the 1064 nm laser irradiation was performed (n=5).

**Figure S21**

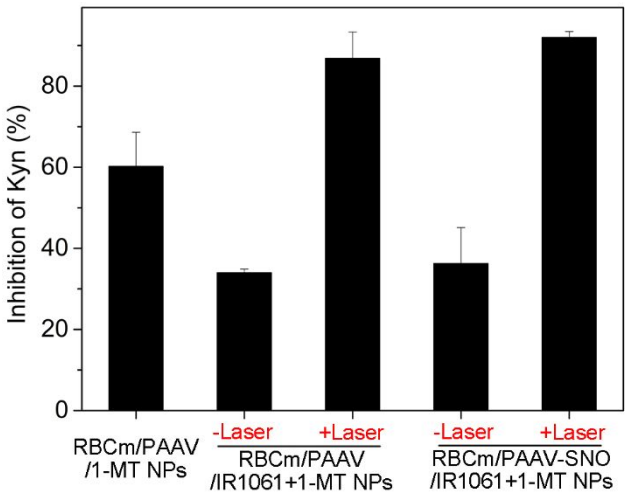


**Figure S21.** Kyn translate inhibition efficiency of different drug formulation with or without 1064 nm laser irradiation (0.86 W/cm$^2$, 5 min) in tumor on day of 12 (n=6).

**Figure S22**

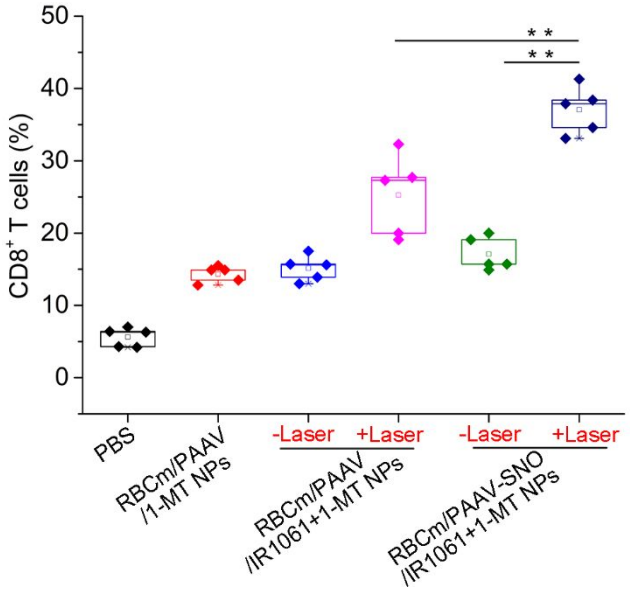


**Figure S22.** CD8+ CTLs frequency in tumor tissue in balb/c mice bearing 4T1 tumors following the indicated treatments on day of 12 (n=6).

**Figure S23**

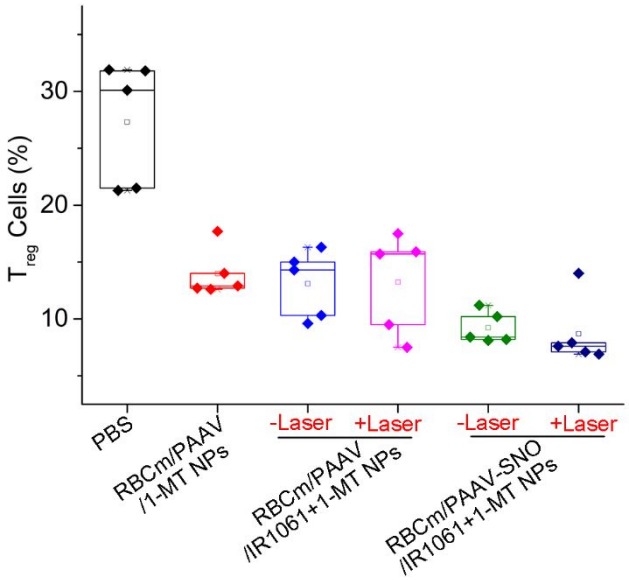


**Figure S23.** Tregs frequency in tumor tissue in balb/c mice bearing 4T1 tumors following the indicated treatments on day of 12 (n=6).

**Figure S24**

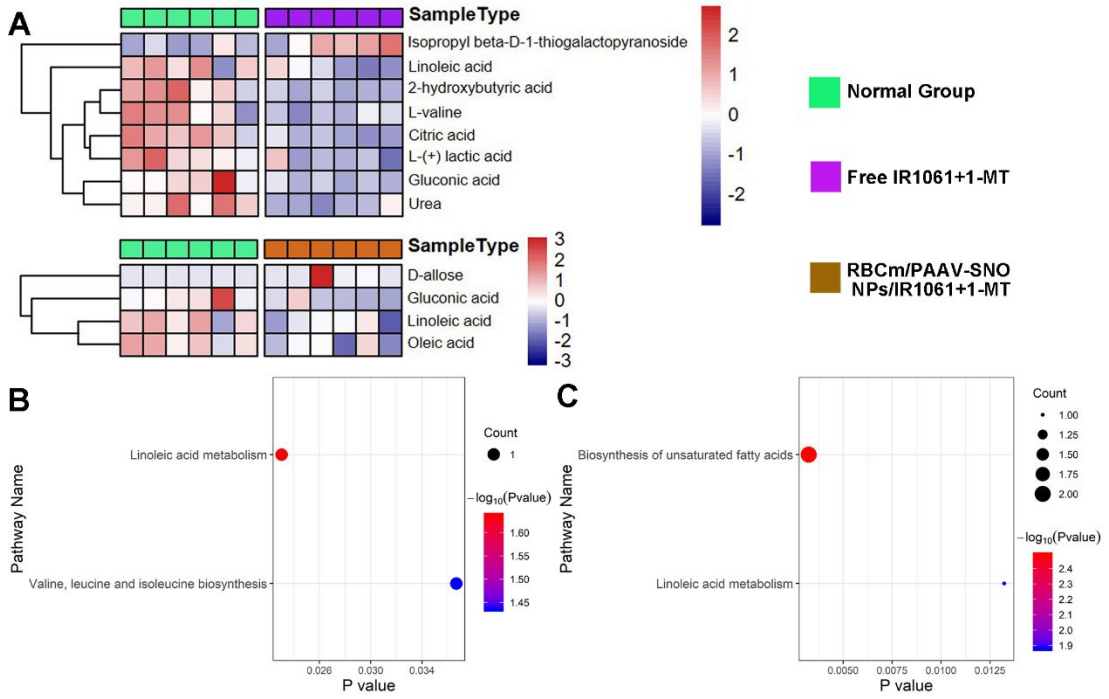


**Figure S24.** (A) Heatmap analysis of metabolites between different drug formulations in plasma. Altered metabolic pathways in plasma of (B) free IR1061+1-MT group *vs.* normal group and (C) RBCm/PAAV-SNO NPs/IR1061+1-MT group *vs.* normal group (n=5).

**Figure S25**

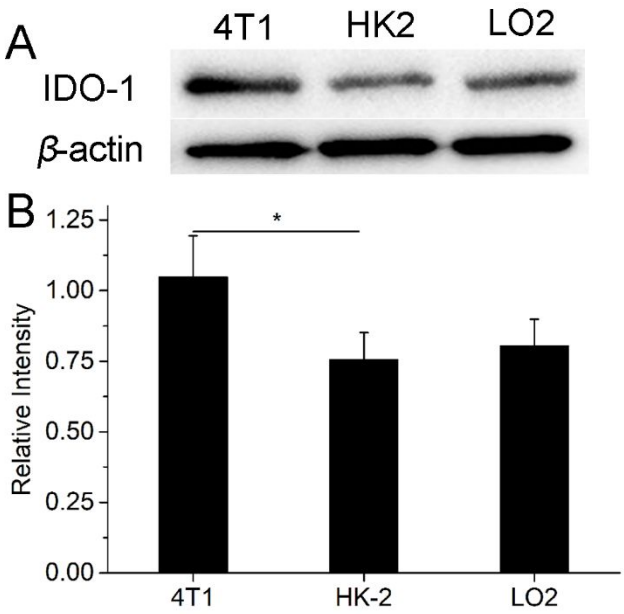


**Figure S25.** (A) Western blot and (B) quantitative analysis of IDO1 protein in total extracts of 4T1, HK-2 and LO2 cells. (n=3)